Composite cores of monopoles and Alice rings in spin-2 Bose-Einstein condensates

Giuseppe Baio⬤ and Magnus O. Borgh⬤

Physics, Faculty of Science, and Centre for Photonics and Quantum Science, University of East Anglia, Norwich NR4 7TJ, United Kingdom

We show that energy relaxation causes a point defect in the uniaxial-nematic phase of a spin-2 Bose-Einstein condensate to deform into a spin-Alice ring that exhibits a composite core structure with distinct topology at short and long distances from the singular line. An outer biaxial-nematic core exhibits a spin half-quantum vortex structure with a uniaxial-nematic inner core. By numerical simulation, we demonstrate a dynamical oscillation between the spin-Alice ring and a split-core hedgehog configuration via the appearance of ferromagnetic rings with associated vorticity inside an extended core region. We further show that a similar dynamics is exhibited by a spin-Alice ring surrounding a spin-vortex line resulting from the relaxation of a monopole situated on a spin-vortex line in the biaxial-nematic phase. In the cyclic phase, similar states are shown instead to form extended phase-mixing cores containing rings with fractional mass circulation or cores whose spatial shape reflects the order-parameter symmetry of a cyclic inner core, depending on the initial configuration.

I. INTRODUCTION

Monopoles are pointlike topological excitations emerging in seemingly distant physical systems across a vast range of energy scales. They have attracted considerable attention since Dirac's first construction of a magnetic monopole [1], where the point charge appears at the termination point of a nodal line. Similar states have also been proposed in superconductors [2] and superfluids [3–5], and prepared in a quantum gas [6]. Monopoles as isolated point singularities are found in theoretical contexts ranging from proposed magnetic monopoles [7,8] in grand unified theories [9–11], to their analogues in condensed-matter systems such as superfluid liquid ^{3}He [3], chiral superconductors [2], and liquid crystals [12–14], as well as in atomic quantum gases [15,16], where they have also been realized [17].

Despite the very different physical contexts, topologically stable monopoles nevertheless exhibit universal fundamental properties that arise generically from underlying symmetries [18,19]. Their pointlike cores are not generally stable, but deform in similar ways into closed line defects: In the context of non-Abelian gauge theories, the core of a 't Hooft-Polyakov monopole [7,8] is predicted to continuously relax into a ring-shaped line defect referred to as an Alice ring [20,21]. Observed far from the core, the configuration still preserves the original monopole charge in the form of a "Cheshire charge" which does not have a localized source, either at any particular point or on the Alice ring [22]. For the same topological reasons, the corresponding point defects in liquid crystals, and atomic quantum gases can similarly deform into

Alice rings in the form of disclination loops [12,13] and closed half-quantum vortices (HQVs) [16], respectively. The Alice ring (closed Alice string) is universally defined by exhibiting a π-winding of a suitably defined order parameter in such a way that a monopole transforms into an antimonopole after one revolution around a loop through the ring [19,20,23–25].

While magnetic monopoles in their original contexts remain elusive [26], analogues of both Dirac and 't Hooft-Polyakov monopoles have recently been realized through controlled preparation [6,17] in spinor Bose-Einstein condensates (BECs) [27,28], using the quadrupole-field imprinting method proposed in Ref. [5] (a three-dimensional generalization of the corresponding vortex-creation method [29,30]). Spinor BECs are created in optical traps that avoid freezing out the spin degree of freedom of the constituent atoms [31], resulting in a multicomponent condensate wave function. Their several magnetic phases exhibit different broken symmetries that provide a rich variety of topological excitations [27,32], which, in addition to monopoles, includes singular [33–41] and nonsingular [42–44] vortices and three-dimensional (3D) skyrmions [45–49]. A long series of experiments realizing vortex nucleation in phase transitions [50], realization of HQVs [51], as well as the controlled creation of 2D [52–54] and 3D [55] skyrmions, singular vortices representing both continuous and discrete symmetries [56–58], and knots [59,60] have established spinor-BECs as robust platforms to investigate topological defects and related textures. It has recently been theoretically proposed [61] and experimentally demonstrated [60] how similar complex topological objects may be optically created in atomic ensembles. In particular, spinor-BECs have proven to be fertile ground for the exploration of the properties, dynamics, and decay of imprinted monopoles [62,63]. The Alice ring resulting from the deformation of a point defect in the polar phase of a spin-1 BEC [16] was recently experimentally observed [63]. This experimental development has been paralleled by

vigorous theoretical work, generalizing the theory of unknotted closed vortices [64] to a rigorous topological description of monopoles and Alice rings [19], as well as analyzing the dynamics of imprinted monopole configurations in spin-1 BECs [65–69].

Here we show how the relaxation of a point defect in the uniaxial-nematic (UN) phase of a spin-2 BEC leads to the formation of a composite-core spin-Alice ring. The expansion of a point defect into an Alice ring happens as a consequence of the "hairy ball" theorem [16] as the core fills with superfluid in a different magnetic phase. We find that the resulting spin-Alice ring develops a biaxial-nematic (BN) outer core, which itself exhibits a spin-HQV structure with a (vortex-free) UN inner core. The spin-Alice ring is therefore an example of a composite defect, which exhibits a hierarchy of different broken symmetries at different length scales such that the core of a singular defect itself harbors a nontrivial defect or texture [70,71]. By numerically simulating its dynamics, we find a dynamical oscillation of the core structure between the spin-Alice ring and a split-core hedgehog configuration [72,73]. Transitions between these states occur via ferromagnetic (FM) rings carrying mass circulation appearing internally in the extended core, separating out from the spin-Alice ring state, and later reemerging from the split-core endpoints with opposite circulation, and eventually returning to approximately the original configuration.

Monopole configurations are also possible in the BN phase, where they occur similarly to Dirac monopoles with associated line defects. Also, these relax to form spin-HQV ring configurations [41]. Here we specifically consider the case of an initial monopole attached to a spin-vortex line extending away from the monopole in both directions. We find that the monopole texture relaxes into a spin-HQV ring surrounding the spin-vortex line, and again exhibits dynamical oscillations between the spin-HQV ring and a split-core configuration. Finally, we similarly consider monopole textures in the cyclic phase. In the case where the spin-vortex line extends away from the monopole in both directions, we find two separated ferromagnetic rings with associated fractional mass circulation, while a nonaxisymmetric core arises when the monopole forms the termination point of one line defect.

This article is organized as follows: In Sec. II, we briefly review the mean-field theory of the spin-2 BEC and relevant topological features of its magnetic phases. In Sec. III, we construct the UN monopole solution and analyze its energy relaxation and the dynamics of the resulting state. In Sec. IV, we more briefly describe energy relaxation and dynamics resulting from a BN monopole as well as energy relaxation of monopoles in the cyclic phase, before short concluding remarks in Sec. V.

II. MEAN-FIELD THEORY AND TOPOLOGY

The spin-2 BEC is described in the Gross-Pitaevskii mean-field theory by a five-component wave function $\Psi(\mathbf{r}) = \sqrt{n(\mathbf{r})}\zeta(\mathbf{r})$, which we decompose into the atomic density $n(\mathbf{r}) = \Psi^\dagger(\mathbf{r})\Psi(\mathbf{r})$ and a normalized spinor $\zeta(\mathbf{r}) = [\zeta_2(\mathbf{r}), \ldots, \zeta_{-2}(\mathbf{r})]^{\mathrm{T}}$ satisfying $\zeta^\dagger(\mathbf{r})\zeta(\mathbf{r}) = 1$. The mean-field

Hamiltonian density is then [27]

$$\mathcal{H}[\Psi] = \Psi^\dagger \hat{h}_0 \Psi + \left(\frac{c_0}{2} + \frac{c_1|\langle\hat{\mathbf{F}}\rangle|^2}{2} + \frac{c_2|A_{20}|^2}{2} \right) n^2, \quad (1)$$

where $\hat{h}_0 = -\hbar^2\nabla^2/2M + M\omega^2\mathbf{r}^2/2 - p\hat{F}_z + q\hat{F}_z^2$, with M being the atomic mass, ω the angular frequency of an isotropic harmonic trap, and p, q linear and quadratic Zeeman shifts [74], which we neglect from this point on. The interaction strengths $c_{0,1,2}$ are obtained from the two-particle s-wave scattering lengths a_f as $c_0 = 4\pi\hbar^2(3a_4 + 4a_2)/7M$, $c_2 = 4\pi\hbar^2(a_4 - a_2)/7M$ and $c_4 = 4\pi\hbar^2(3a_4 - 10a_2 + 7a_0)$, where f is the total angular momentum of the colliding atoms [75]. The first two contributions in Eq. (1) are spin-independent and spin-dependent contact interactions, where the condensate spin $\langle\hat{\mathbf{F}}\rangle = \zeta^\dagger\hat{\mathbf{F}}\zeta$ is found from the vector $\hat{\mathbf{F}}$ of spin-2 matrices. The third term depends on the formation amplitude of spin-singlet pairs,

$$A_{20} = \frac{1}{\sqrt{5}}(\zeta_0^2 - 2\zeta_{-1}\zeta_1 + 2\zeta_{-2}\zeta_2). \quad (2)$$

In the absence of Zeeman shifts, the spin-2 BEC exhibits four topologically distinct, uniform ground-state phases. Two energetically degenerate, but distinct and individually dynamically stable nematic phases with $|\langle\hat{\mathbf{F}}\rangle| = 0$ and $|A_{20}| = \sqrt{1/5}$ form ground states in a uniform system when $c_1 > 0$ and $c_2 < 0$, and for $c_1 < 0$ when $c_2 < 20c_1$ [27]. The first of these is the UN phase, which can be represented by the spinor

$$\zeta^{\mathrm{UN}} = (0, 0, 1, 0, 0)^{\mathrm{T}}. \quad (3)$$

The symmetry of the order parameter can be illustrated using the spherical-harmonics representation,

$$Z(\theta, \varphi) = \sum_{m=-2}^{2} Y_{2,m}(\theta, \varphi)\zeta_m, \quad (4)$$

where θ and φ are local spherical coordinates. Applying this representation to Eq. (3) yields Fig. 1(a), showing the symmetry axis $\hat{\mathbf{d}}$. Any other UN spinor can be constructed by applying a shift of the condensate phase (gauge) τ [an element of U(1)] and a 3D spin rotation [an element of SO(3)], parametrized by three Euler angles α, β, γ as

$$\zeta \rightarrow e^{i\tau} \exp(-i\alpha\hat{F}_z) \exp(-i\beta\hat{F}_y) \exp(-i\gamma\hat{F}_z)\zeta. \quad (5)$$

This transformation represents the full symmetry group $G = \mathrm{U}(1) \times \mathrm{SO}(3)$ of Eq. (1). The isotropy group H of elements of G that leave the spinor unchanged yields the order parameter manifold as $\mathcal{M} = G/H$ [18]. Specifically, it follows from Fig. 1(a) that ζ^{UN} is unchanged by any rotation about the nematic axis $\hat{\mathbf{d}}$, and also by taking $\hat{\mathbf{d}} \rightarrow -\hat{\mathbf{d}}$ (nematic symmetry). As a result, the UN order-parameter space is $\mathcal{M}^{\mathrm{UN}} = U(1) \times (S^2/\mathbb{Z}_2)$, where S^2 is the 2-sphere [76].

By contrast, the second stationary, nematic solution (with the same $|\langle\hat{\mathbf{F}}\rangle|$ and $|A_{20}|$) is the BN phase represented by

$$\zeta^{\mathrm{BN}} = \frac{1}{\sqrt{2}}(1, 0, 0, 0, 1)^{\mathrm{T}}, \quad (6)$$

whose spherical-harmonics representation is shown in Fig. 1(b). The isotropy group is now described by the fourfold
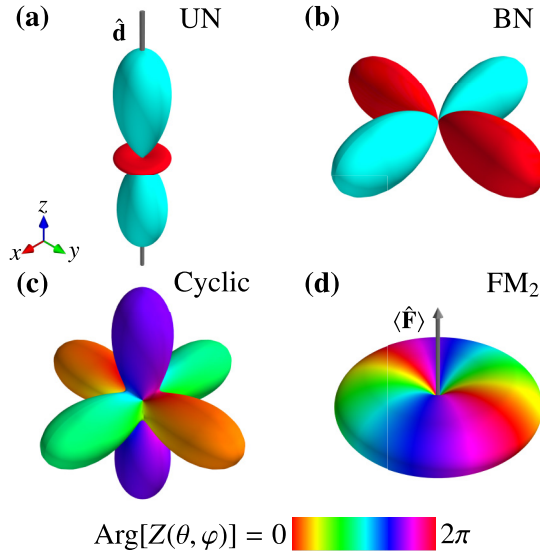
FIG. 1. Spherical-harmonics representations [Eq. (4)] for representative spinors of spin-2 magnetic phases. (a) UN phase, with order parameter given by an unoriented nematic axis $\hat{\mathbf{d}}$ and the condensate phase. (b) BN phase, exhibiting a discrete fourfold dihedral symmetry that combines with the condensate phase. (c) Cyclic phase, with tetrahedral symmetry combined with the condensate phase. (d) FM$_2$ phase, whose order parameter is related to rotations in three dimensions. The arrow indicates the corresponding condensate spin vector $\langle \mathbf{F} \rangle$.

dihedral subgroup of SO(3) combined with π-shifts of τ, together denoted $(D_4)_{\tau,\mathbf{F}}$, leading to the manifold $\mathcal{M}^{\mathrm{BN}} = G/(D_4)_{\tau,\mathbf{F}}$ [41,77–79]. In addition to the different order-parameter symmetry (and therefore distinct topology), the two nematic states can be further distinguished by the amplitude of spin-singlet trio formation,

$$A_{30} = \frac{3\sqrt{6}}{2}(\zeta_1^2 \zeta_{-2} + \zeta_{-1}^2 \zeta_2) + \zeta_0(\zeta_0^2 - 3\zeta_1\zeta_{-1} - 6\zeta_2\zeta_{-2}), \tag{7}$$

such that $|A_{30}| = 1$ for the UN and $|A_{30}| = 0$ for the BN phases [80].

Based on measurements of the *s*-wave scattering lengths, the nematic phases are predicted to form the uniform ground state for commonly used atoms such as ^{87}Rb [81–83] and ^{23}Na [81]. Beyond mean-field level, the energetic degeneracy of the two phases can be lifted by zero-point quantum fluctuations, which yield higher-order corrections to Eq. (1). These favor either the UN or the BN phase depending on parameters and have been calculated, e.g., for ^{87}Rb in an optical lattice [78] and for uniform nematic condensates of both ^{87}Rb and ^{23}Na [84]. The degeneracy can also be explicitly broken already at the mean-field level through a nonzero quadratic Zeeman level shift [41]. However, including Zeeman shifts in Eq. (1) also leads to further, parameter-dependent stationary solutions [75,85,86] and restricts the symmetry group G [27] (though this effect is negligible for sufficiently small level shifts). For our purposes, the mean-field dynamical stability of each nematic phase even in the absence of level shifts is sufficient.

When $c_1, c_2 > 0$, the cyclic phase with representative spinor,

$$\zeta^{\mathrm{C}} = \frac{1}{\sqrt{2}}\left(1, 0, i\sqrt{2}, 0, 1\right)^{\mathrm{T}}, \tag{8}$$

whose spherical-harmonics representation is shown in Fig. 1(c), instead becomes the uniform ground state. The interaction contributions now imply $|\langle \hat{\mathbf{F}} \rangle| = |A_{20}| = 0$. The isotropy group here is described by combinations of elements of the tetrahedral subgroup of SO(3) with $2\pi/3$-shifts of the condensate phase, together denoted $(T)_{\tau,\mathbf{F}}$. The order parameter manifold is correspondingly $\mathcal{M}^{\mathrm{C}} = G/(T)_{\tau,\mathbf{F}}$ [38,77].

Finally, when $c_1 < 0$ and $c_2 > 20c_1$, energy minimization in the uniform system requires maximizing the condensate spin, yielding a FM phase, FM$_2$, with $|\langle \hat{\mathbf{F}} \rangle| = 2$ and $|A_{20}| = 0$, represented by

$$\zeta^{\mathrm{FM}_2} = (1, 0, 0, 0, 0)^{\mathrm{T}}, \tag{9}$$

whose symmetry is shown in Fig. 1(d), with an order-parameter space corresponding to 3D rotations [58,87].

Topological defects in ordered media are classified through the homotopy groups of the order-parameter manifold [18]. In three dimensions, the first homotopy group $\pi_1(\mathcal{M})$, whose elements are the classes of maps of closed loops into $\mathcal{M}$, identifies singular line defects. Similarly, considering maps of closed surfaces into $\mathcal{M}$ yields the second homotopy group $\pi_2(\mathcal{M})$, which characterizes topologically stable point defects. It can also describe topological charges of nonsingular textures whose boundary conditions are fixed, such as 2D skyrmions. In the spin-2 BEC, only the UN phase exhibits a nontrivial second homotopy group, $\pi_2(\mathcal{M}^{\mathrm{UN}}) = \mathbb{Z}$. Its integer elements correspond to the monopole charge [18,25], counting how many times surfaces enclosing the point defects span the manifold $\mathcal{M}^{\mathrm{UN}}$ in the mapping. For all other spin-2 phases, $\pi_2(\mathcal{M}) = 0$, i.e., the second homotopy group is trivial, and there are consequently no topologically protected, singular point defects. However, they still exhibit solutions corresponding to monopoles attached to one or more singular defect lines [41,88], in analogy with Dirac's construction [1]. In the FM case, this leads to the spin-2 generalization of the Dirac monopoles in the FM phase of spin-1 BECs [4], and can still be characterized by a well-defined winding number as long as the boundary conditions on the spin texture are fixed. This construction also generalizes to the BN [41] and cyclic phases in spin-2 BECs.

Relaxation and dynamical stability of the solutions are investigated via the coupled Gross-Pitaevskii equations,

$$i\hbar\frac{\partial\Psi}{\partial t} = \left[\hat{h}_0 + (c_0 + c_1\langle \hat{\mathbf{F}} \rangle \cdot \hat{\mathbf{F}})n + \frac{c_2}{5}(\hat{\mathcal{T}}\Psi)^{\dagger}\Psi\hat{\mathcal{T}}\right]\Psi, \tag{10}$$

obtained from the energy functional in Eq. (1). Here the operator $\hat{\mathcal{T}}$ is defined as $(\hat{\mathcal{T}}\Psi)_m = (-1)^m \Psi_{-m}^*$ such that $nA_{20} = (\hat{\mathcal{T}}\Psi)^{\dagger}\Psi/\sqrt{5}$ [89]. Equations (10) are integrated using a split-step method [90] on a Cartesian grid of 128^3 points. Interaction-strength ratios are chosen as $c_0/c_1 = 90.7$, $c_0/c_2 = -102$, with $Nc_0 = 1.32 \times 10^4 \hbar\omega\ell^3$, corresponding to $N = 2 \times 10^5$ ^{87}Rb atoms in a trap with angular frequency $\omega = 2\pi \times 130$ Hz [82]. Here $\ell = (\hbar/M\omega)^{1/2}$ is the oscillator

length. We focus on the relaxation routes of monopole solutions in the dynamically stable UN, BN, and cyclic phases. To determine these, we first propagate the solutions in imaginary time, i.e., taking $t \to it$ in Eq. (10). Dynamical stability of the relaxed cores is probed by subsequent forward propagation, where time is taken to include a small imaginary component, $t \to (1 - i\nu)t$, to phenomenologically account for dissipation. The damping coefficient is chosen as $\nu \approx 10^{-2}$, which has previously been found to model experimental observations well [56–58]. Our results are qualitatively insensitive to small variations of ν. We neglect Zeeman shifts, though also in this case, a sufficiently weak quadratic shift (to break energetic degeneracy) does not qualitatively change our results.

III. UNIAXIAL-NEMATIC MONOPOLE AND COMPOSITE-CORE ALICE RING

An isolated monopole in the UN phase is constructed by taking the nematic axis to coincide with the radius vector everywhere, i.e., $\hat{\mathbf{d}} = \hat{\mathbf{r}} = \cos\varphi \sin\theta\, \hat{\mathbf{x}} + \sin\varphi \sin\theta\, \hat{\mathbf{y}} + \cos\theta\, \hat{\mathbf{z}}$, where (θ, φ) are spherical coordinates centered on the singular point. Since the state with $\hat{\mathbf{d}} = \hat{\mathbf{z}}$ is exactly Eq. (3), we can immediately apply Eq. (5) with Euler angles $\alpha = \varphi$, $\beta = \theta$ and condensate phase $\tau = 0$ to find

$$\zeta_{\mathrm{pm}}^{\mathrm{UN}} = \sqrt{\frac{3}{8}} \begin{pmatrix} e^{-2i\varphi} \sin^2\theta \\ -e^{-i\varphi} \sin 2\theta \\ \frac{1}{\sqrt{6}}(1 + 3\cos 2\theta) \\ e^{i\varphi} \sin 2\theta \\ e^{2i\varphi} \sin^2\theta \end{pmatrix}. \quad (11)$$

Note that the third Euler angle γ drops out and does not need to be specified. In exact analogy with the isolated-monopole solution in the spin-1 polar phase [16] as well as point defects in superfluid liquid ^{3}He and nematic liquid crystals [25], a topologically protected charge $W_{\hat{\mathbf{d}}}$ can now be defined as

$$W_{\hat{\mathbf{d}}} = \frac{1}{4\pi} \int_{S^2} d\theta d\varphi\, \hat{\mathbf{d}} \cdot \left(\frac{\partial \hat{\mathbf{d}}}{\partial \theta} \times \frac{\partial \hat{\mathbf{d}}}{\partial \varphi} \right). \quad (12)$$

Note that since $\hat{\mathbf{d}}$ is unoriented, the sign of $W_{\hat{\mathbf{d}}}$ is arbitrary and the charge of the monopole is properly given by $|W_{\hat{\mathbf{d}}}|$.

Isolated-monopole solutions are characterized by an energetically costly core where the superfluid density is depleted and whose size is determined by the density healing length $\xi_n = \ell(\hbar\omega/2nc_0)^{1/2}$ [15]. In spinor BECs, however, defect cores can lower their energy by filling with atoms in a different magnetic phase [16,35]. In a spin-2 BEC, the condensate may therefore instead break conditions on $|\langle \hat{\mathbf{F}} \rangle|$ or $|A_{20}|$. The size of the defect core is then instead determined by the spin healing length $\xi_F = \ell(\hbar\omega/2n|c_1|)^{1/2}$ in the former case, or the singlet healing length $\xi_a = \ell(\hbar\omega/2n|c_2|)^{1/2}$ in the latter. Since, typically, $|c_1|, |c_2| \ll c_0$, and ξ_F and ξ_a correspondingly larger than ξ_n, the filled core expands such that the increased interaction energy inside the core is offset by a lower kinetic contribution due to the smaller gradients. In spin-2, one further possibility arises however: a UN defect singularity can also be accommodated by atoms in the BN phase, or vice versa. Since both nematic phases are energetically degenerate at the mean-field level, unless continuity of the wave function causes mixing with other phases to arise

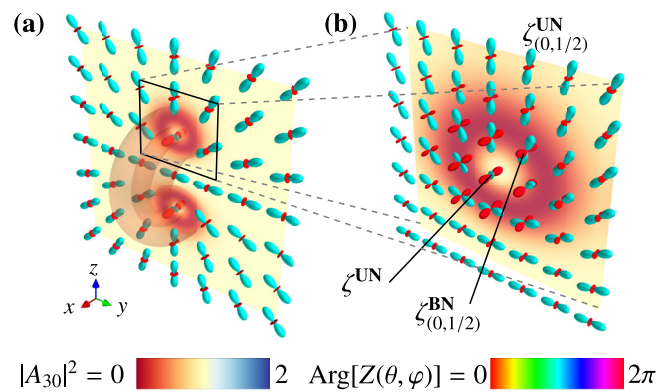$|A_{30}|^2 = 0$ [color bar] 2 $\mathrm{Arg}[Z(\theta,\varphi)] = 0$ [color bar] 2π

FIG. 2. Composite-core spin-Alice ring in the UN phase. (a) Ring defect structure with spin-HQV charge obtained after imaginary-time propagation at $\omega t \approx i\pi$, shown by $|A_{30}|^2$ in the yz plane (color map), and isosurfaces at $|A_{30}|^2 = 1/2$. The local order parameter is shown in the yz plane using the spherical-harmonics representation. (b) Detail of the spin-Alice ring core, showing the outer BN core with spin-HQV structure and the inner UN core.

in the core [41,88], no interaction-energy condition is broken and so the size of the core is, in principle, not constrained by any healing length.

For the UN point defect, however, similarly to its analogue in polar spin-1 BECs [16] and 't Hooft-Polyakov monopoles [20,21], the filling of its core while maintaining spherical symmetry would imply the existence of a vector field identified by a different local symmetry axis orthogonal to $\hat{\mathbf{d}}$ and thus tangent to S^2, which for a point-defect core would violate the "hairy ball" theorem. Instead, the singular locus continuously deforms into a closed line defect, shown by numerical energy relaxation in Fig. 2(a). Here we make use of the spherical-harmonics representation (4) to illustrate the resulting $\hat{\mathbf{d}}$-field. On any surface enclosing the line-defect ring, the charge $W_{\hat{\mathbf{d}}}$ is left unchanged, while $\hat{\mathbf{d}}$ now penetrates the center of the texture. Along any loop passing through the defect ring, $\hat{\mathbf{d}}$ transforms into $-\hat{\mathbf{d}}$. In contrast to the spin-1 case, but similarly to nematic liquid crystals, the $\mathbb{Z}_2$ symmetry of the UN order parameter is decoupled from the condensate phase τ, and so the condensate wave function Ψ remains single valued everywhere without any compensatory phase winding that would lead to mass circulation. The closed line defect resulting from relaxation of the point defect is therefore a spin HQV, analogous to π-disclination loops in nematic liquid crystals [12,13]. Further, the spin HQV is a spin-Alice ring: in a UN, a monopole of charge $|W_{\hat{\mathbf{d}}}| = 1$ turns into its own antimonopole precisely when encircling a spin HQV [25], establishing the property [19].

While in the spin-1 case a singular defect in a polar phase can only develop a ferromagnetic core (and vice versa), the much larger family of stationary states in spin-2 BECs allows the same singular defect to develop very different filled cores depending on parameters [41], experimental choice [58], or defect configurations [88]. The resulting core structure may develop considerable complexity as a result of the interplay between continuous and polytope order-parameter symmetries. Figure 2 shows how the spin-Alice ring resulting from the relaxation of the UN point defect develops

a composite core structure, characterized by a hierarchy of topologically different phases on small and large distances, such that the core of the defect itself exhibits a vortex structure [70,71]. Specifically, the order parameter interpolates smoothly between the the UN and BN phases, from the UN bulk containing the spin-HQV ring, through a BN outer core (characterized by vanishing $|A_{30}|^2$), which itself exhibits a spin-HQV structure [Fig. 2(b)]. This, in turn, exhibits a (non-rotating) UN core that forms the inner core of the spin-Alice ring. The topology of the inner and outer cores and the bulk connect by deforming the order parameter along different axes, such that the axis of spin rotation that defines the UN and BN spin HQVs coincides with one of the symmetry axes of the BN order parameter. This formation of a BN region surrounding a UN ring is closely similar to predictions for a point defect in a nematic liquid crystal confined to a cylindrical capillary tube [91].

The transitions within the composite core provide an example of a state with two topological interfaces [56,58,71,92,93], for which interpolating model wave functions that connect the vortex states can be explicitly constructed [88]. At any point on the vortex spin-HQV line, we may define local cylindrical coordinates and construct the phase-mixing spinor,

$$\zeta_{(0,1/2)}^{\text{UN-BN}} = \frac{1}{\sqrt{2}}\big[D_+(\rho)\zeta_{(0,1/2)}^{\text{UN}} - D_-(\rho)\zeta_{(0,1/2)}^{\text{BN}}\big], \quad (13)$$

where

$$\zeta_{(0,1/2)}^{\text{UN}} = \frac{1}{\sqrt{8}}\big(\sqrt{3}e^{-i\varphi}, 0, -\sqrt{2}, 0, \sqrt{3}e^{i\varphi}\big)^{\text{T}}, \quad (14)$$

$$\zeta_{(0,1/2)}^{\text{BN}} = \frac{1}{\sqrt{8}}\big(e^{-i\varphi}, 0, \sqrt{6}, 0, e^{i\varphi}\big)^{\text{T}}, \quad (15)$$

and $D_\pm(\rho) = [1 \pm f(\rho)]^{1/2}$ for a suitable interpolating function $f(\rho)$ of the radial distance. Equations (14) and (15) are obtained, respectively, from Eqs. (3) and (6) under the transformation (5) with $\tau = 0$, $\alpha = \varphi/2$, and $\beta = \pi/2$. The result in each case is a spin HQV with no mass circulation, which we denote by the subscript $(0, 1/2)$. Expressions of the form of Eq. (13) are very general and can describe several different UN-BN topological-interface structures [88], including filled vortex cores. For Eq. (13) specifically, taking $f(\rho) \to \pm1$ yields, respectively, the UN and BN spin HQVs. Additionally, for $f(\rho) = \pm1/2$, we recover a further BN spin HQV (+) and the vortex-free UN (−) spinor. The composite core structure, depicted in Fig. 2(b), can thus be parametrized by taking $f(\rho)$ to vary smoothly from $f(0) = -1/2$ on the vortex line (inner UN core), via $f(\rho^*) = 1/2$ in the BN outer core at some distance ρ^* from the singular line, to $f(\rho) \to 1$ for the UN spin HQV outside the core region. Since the interaction energy is unchanged between the UN and BN phases, the size of the Alice ring can expand very rapidly during energy relaxation.

In order to study its dynamics, we now numerically propagate the spin-Alice ring state in Fig. 2 forward in time, which we give a small imaginary part to phenomenologically account for dissipation. We find that the spin-Alice ring core exhibits a dynamical oscillation, shown in Fig. 3, characterized by the appearance of a pair of FM rings, originating from the spin-Alice ring, with an associated mass circulation. The vorticity structure can be unpacked by introducing two
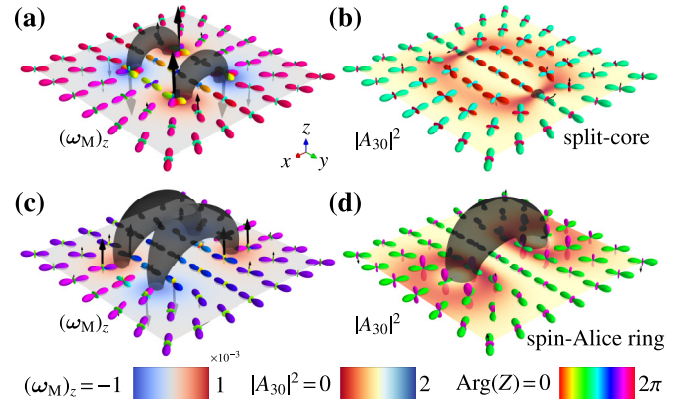

FIG. 3. Core oscillations of a spin-Alice ring, shown by frames of complex-time simulation. (a) Separation of two vortex rings with FM core at $\omega t \approx 3.2$. (b) Vortex rings collapse into the split-core configuration at $\omega t \approx 7.5$. (c) Vortex rings reemerge with opposite mass circulation at $\omega t \approx 10.5$. (d) Retrieval of the spin-Alice ring (single ring with maximal spin vorticity) at $\omega t \approx 15$. All panels show the local $\langle\hat{\mathbf{F}}\rangle$ (black arrows), spherical-harmonics representation of the order parameter, and isosurfaces of the spin-summed pseudovorticity magnitude. In (a) and (c), mass circulation is indicated by the z component of the mass pseudovorticity (color map). In (b) and (d), the color map indicates $|A_{30}|^2$, showing the two nematic core structures of the split-core and spin-Alice ring states, respectively.

pseudovorticity vector fields [94,95] measuring the local circulation of the mass and spin supercurrents and defined as [27,32]

$$\boldsymbol{\omega}_{\text{M}} = -\frac{i\hbar}{2M}\nabla \times \sum_{\mu=-2}^{2}\big(\psi_\mu^*\nabla\psi_\mu - \psi_\mu\nabla\psi_\mu^*\big), \quad (16)$$

$$\boldsymbol{\omega}_{\text{S}}^\alpha = -\frac{i\hbar}{2M}\nabla \times \sum_{\mu,\nu}(\hat{F}_\alpha)_{\mu,\nu}\big(\psi_\mu^*\nabla\psi_\nu - \psi_\nu\nabla\psi_\mu^*\big), \quad (17)$$

where $\alpha = x, y, z$. We visualize the mass vorticity in a plane orthogonal to the initial spin-Alice ring orientation in Fig. 2(a). We choose the plane $z = 0$, where $\boldsymbol{\omega}_{\text{M}}$ is approximately aligned with the z axis. Plotting its z component, we identify regions of nonvanishing mass circulation surrounding the points where $|\langle\hat{\mathbf{F}}\rangle|$ becomes appreciable. Moreover, the rings exhibit spin circulation, which we visualize by defining the scalar quantity $\sum_\alpha |\boldsymbol{\omega}_{\text{S}}^\alpha|^2$ (i.e., the sum of the magnitude squared of the x, y, z spin pseudovorticities) as a measure of the total spin circulation. This is shown as 3D isosurfaces in Fig. 3(a), indicating maximal spin vorticity in two distinct rings. The configuration corresponds to an extended core region associated with the monopole charge, containing the singularity of the bulk UN order parameter.

Quickly after separation, the radii of the spin-vorticity rings shrink, reducing the corresponding singularities of the UN order parameter to density-depleted points, joined by a segment where the UN order parameter takes the opposite sign, as shown in Fig. 3(b). This configuration corresponds to the split-core hedgehog, introduced as a further relaxation channel for 't Hooft-Polyakov monopoles in high-energy physics [21] and point defects in nematic liquid crystals [72,73]. The vortex rings later reemerge from the split-core

endpoints with opposite circulation and drift direction, as shown in Fig. 3(c), and eventually overlap to once again form the spin-Alice ring, as shown in Fig. 3(d). The oscillation pattern repeats with a period of $\sim 2\pi \times 2.5\omega^{-1}$. By tracing $\mathrm{Arg}(Z)$ in the spherical-harmonics representation of the spinor [Eq. (4)], we determine that the condensate phase τ winds by π on a path around any one vortex ring in Figs. 3(a) and 3(c). Since the condensate spin vanishes outside the FM ring, the mass current depends only on τ [27], and so this corresponds to the mass circulation of an HQV. However, as shown in Figs. 3(a) and 3(c), the vortex rings are embedded within the phase-mixing extended core structure, such that no closed path through one (or both) of the FM rings exhibits a single magnetic phase. Neither ring can therefore be understood as a well-defined topological defect in its own right.

IV. STRUCTURE AND DYNAMICS OF MONOPOLE CORES IN THE BIAXIAL-NEMATIC AND CYCLIC PHASES

A. Biaxial-nematic monopoles and vortex-ring formation

Although $\pi_2(\mathcal{M}^{\mathrm{BN}}) = 0$, we can explicitly construct solutions in the BN phase where a monopole texture is attached to a line defect that extends away in opposite directions from the center of the monopole. In particular, we can construct a radial hedgehog by aligning one of the symmetry axes of the BN order parameter (cf. Fig. 1) with the radius vector [41]. Here we choose one of the twofold principal axes: Starting from the spinor

$$\zeta^{\mathrm{BN}} = \frac{1}{\sqrt{8}}\left(1, 0, \sqrt{6}, 0, 1\right)^{\mathrm{T}} \tag{18}$$

[related to Eq. (6) by a $\beta = \pi/2$ rotation], we apply Eq. (5) with $\alpha = \varphi$ and $\beta = \theta$ ($\tau = \gamma = 0$) to form the hedgehog. The resulting state is similar to that introduced in liquid crystals to describe the BN ordering around an anchoring colloid [96] and is described by the spinor

$$\zeta^{\mathrm{BN}}_{1\text{-pm-1}} = \frac{1}{\sqrt{8}}\begin{pmatrix} e^{-2i\varphi}(1+\sin^2\theta) \\ -e^{-i\varphi}\sin 2\theta \\ \sqrt{6}\cos^2\theta \\ e^{i\varphi}\sin 2\theta \\ e^{2i\varphi}(1+\sin^2\theta) \end{pmatrix}. \tag{19}$$

Energy relaxation of monopole solutions in the BN phase leads to different core structures depending on the initial configuration of the hedgehog and associated line defects [41]. Imaginary-time propagation of the Gross-Pitaevskii equations starting from Eq. (19) results in the formation of a spin-HQV ring defect, emerging from the hedgehog texture, that encircles the singly quantized spin vortex along the z axis. The cores of both defects fill with atoms in the UN phase, as shown in Fig. 4(a). The ring defect exhibits spin circulation, again indicated by an isosurface of $\sum_\alpha |\boldsymbol{\omega}_{\mathrm{S}}^\alpha|^2$ showing the region of maximal spin pseudovorticity as defined in Eq. (17). The BN spin-HQV ring is similar in structure to the spin-Alice ring in the UN case [comparing Figs. 2 and 4(a)], both exhibiting the inversion of an unoriented axis on closed loops around the singular line, without the need for any accompanying shift of the condensate phase. In this sense, the BN spin HQV may also be thought of as an Alice ring by analogy, despite
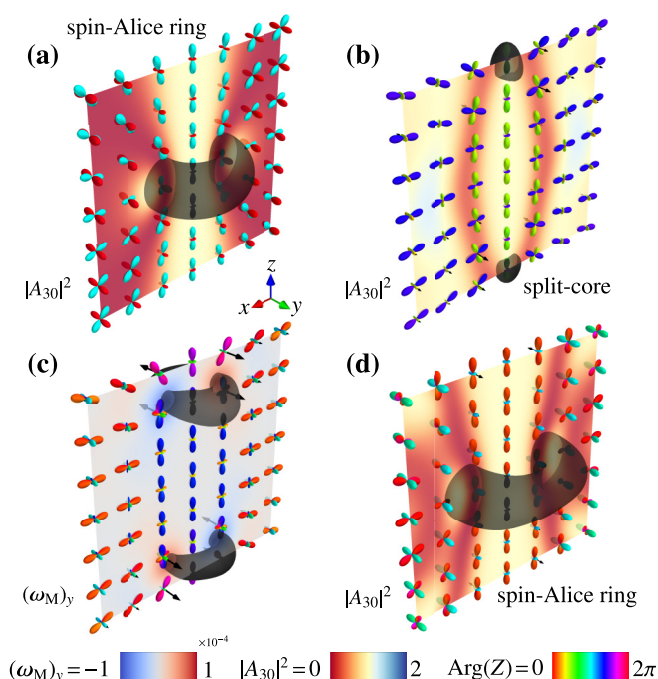

FIG. 4. Core oscillations of a BN spin-Alice ring shown by frames of complex time simulation. (a) Core structure of the BN spin-Alice ring penetrated by a spin vortex along z as the initial state. (b) Split-core-like configuration at $\omega t \approx 12.5$. (c) Vortex rings with mass circulation emerging from the split-core endpoints at $\omega t \approx 14.5$. (d) Retrieval of a spin-Alice ring (single ring with spin vorticity and no mass circulation) at $\omega t \approx 22$. The order parameter is shown by spherical-harmonics representation. The core structures in (a), (b), and (d) are shown by the scalar $|A_{30}|^2$ in the xz plane (color map). In (c), the color map indicates the y component of mass pseudovorticity.

the absence of point defects in the BN phase. The similarity between the BN spin-HQV ring in the BN phase and the UN spin-Alice ring is further emphasized by noting that the core structure of the former may still be locally parametrized using Eq. (14), connecting the spin-HQV-carrying BN bulk order parameter with the UN core across a topological interface. In this case, we take $f(\rho)$ to vary from $f(0) = -1/2$ on the line singularity to $f(\rho) = 1/2$ for sufficiently large ρ to reach the BN phase away from the vortex line.

The BN spin-Alice ring also exhibits a closely similar dynamics to its UN counterpart. Complex-time propagation taking the BN spin-Alice ring plus spin-vortex configuration in Fig. 4(a) as the initial state also results in oscillations of the core structure analogous to Fig. 3. Here these are characterized by a first rapid expansion of the UN core in both the spin-Alice ring and the spin vortex along the z axis, giving rise to separating vortex rings with nonvanishing mass and spin circulation, drifting away from the center of the condensate. Also, similarly to the UN case (Fig. 3), the vortex rings shrink to points of density depletion in a split-core-like configuration [Fig. 4(b)], later reemerging with opposite circulation and inwards drift direction [Fig. 4(c)]. The core structure eventually returns to its original configuration, where the rings overlap to form a BN spin-Alice ring, as shown in Fig. 4(d). Despite the

similar dynamics, however, the BN configuration deteriorates more rapidly with dissipation and, after longer complex-time propagation, the spin-Alice ring is eventually lost.

B. Core structure of a cyclic monopole

We can apply a construction similar to that leading to Eq. (19) to construct a monopole state in the cyclic phase. The second homotopy group $\pi_2(\mathcal{M}^C)$ is again trivial and any monopole must come with associated singular lines. Starting from the representative cyclic spinor in Eq. (8), and applying Eq. (5) with Euler angles $\alpha = \varphi$ and $\beta = \theta$ ($\tau = \gamma = 0$), we obtain

$$\zeta^C_{1\text{-pm-1}} = \frac{1}{8}\begin{pmatrix} e^{-2i\varphi}\big[3 + i\sqrt{3} + 2e^{-i\pi/3}\cos 2\theta\big] \\ 4e^{-i\varphi}e^{-i\pi/3}\sin 2\theta \\ i\sqrt{2}\big(1 + 3\cos 2\theta - 2i\sqrt{3}\sin^2\theta\big) \\ -4e^{i\varphi}e^{-i\pi/3}\sin 2\theta \\ e^{2i\varphi}\big[3 + i\sqrt{3} + 2e^{-i\pi/3}\cos 2\theta\big] \end{pmatrix}, \quad (20)$$

representing a radial hedgehog in one of the three principal symmetry axes of the cyclic order parameter (cf. Fig. 1 situated on a spin vortex extending along the z axis).

It is also possible to construct a monopole solution more similar to the FM Dirac monopoles [4], where the defect line extends away from the monopole in only one direction. In the BN phase, such a monopole was constructed in Ref. [41]. We follow the same method here by adding a spin rotation $\gamma = -\varphi$ in Eq. (5) in the construction of the hedgehog. This has the effect of compensating the effect of the rotations $\alpha = \varphi$ and $\beta = \theta$ in such a way that the cyclic order parameter remains nonsingular everywhere, except for a singly quantized spin vortex along the negative z axis, terminating as the cyclic monopole at the origin. For notational convenience, the resulting spinor can be decomposed as

$$\zeta^C_{1\text{-pm}} = \frac{1}{\sqrt{2}}\big(i\zeta^{UN}_{pm} + \zeta^{BN}_{1\text{-pm}}\big), \quad (21)$$

where ζ^{UN}_{pm} is defined in Eq. (11) and

$$\zeta^{BN}_{1\text{-pm}} = \frac{1}{\sqrt{8}}\begin{pmatrix} 2\big(\cos^4\frac{\theta}{2} + e^{-4i\varphi}\sin^4\frac{\theta}{2}\big) \\ e^{-3i\varphi}\sin\theta\big[\cos\theta - 1 + e^{4i\varphi}(\cos\theta + 1)\big] \\ \sqrt{6}\cos 2\varphi\sin^2\theta \\ -e^{-i\varphi}\sin\theta\big[\cos\theta - 1 + e^{4i\varphi}(\cos\theta + 1)\big] \\ 2\big(\cos^4\frac{\theta}{2} + e^{4i\varphi}\sin^4\frac{\theta}{2}\big) \end{pmatrix} \quad (22)$$

coincides with the analogous construction of a BN monopole as the termination point of a spin vortex.

Considering first energy relaxation of the monopole attached to a spin vortex along the whole z axis, given by Eq. (20), we find, similarly to the BN case [Fig. 4(a)], that the singly quantized spin vortex develops a UN core extending along z. By contrast, however, no surrounding spin-vortex ring emerges from the cyclic hedgehog. Instead, we find the immediate formation of two separated vortex rings with FM core. This is highlighted by the local $\langle\hat{\mathbf{F}}\rangle$ and the isosurfaces with $|\langle\hat{\mathbf{F}}\rangle| = 1$, corresponding to regions with nonzero mass and spin vorticity. Each vortex ring displays a fractional $2\pi/3$-winding of the global phase around the FM core, as highlighted from the spherical harmonics in Fig. 5(a).
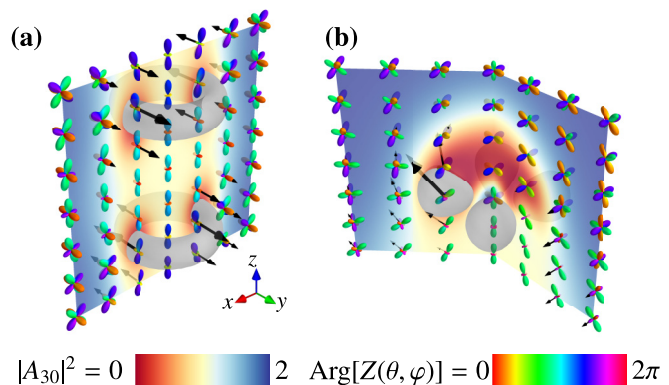

$|A_{30}|^2 = 0$ ▬▬▬ 2 $\text{Arg}[Z(\theta,\varphi)] = 0$ ▬▬▬ 2π

FIG. 5. Relaxed core structures of cyclic monopoles, shown by $|A_{30}|^2$ in the zx plane, spherical-harmonics representation of the order parameter, and isosurfaces corresponding to $|\langle\hat{\mathbf{F}}\rangle| = 1$. (a) Cyclic hedgehog with associated spin vortex [Eq. (20)], showing separated vortex rings with FM core. (b) Cyclic monopole as the termination of a spin vortex [Eq. (22)], showing a nonaxisymmetric core structure with localized FM regions.

A very different core structure emerges from energy relaxation of the cyclic monopole when it forms the termination point of a spin-vortex line, given in Eq. (22). This core structure is shown in Fig. 5(b) and breaks the axisymmetry about the z axis in favor of the fourfold symmetry. This reflects the symmetry of the cyclic order parameter as the cyclic phase appears as an inner core at the center of a now extended, phase-mixing outer core. Specifically, this extended core contains four localized FM regions, shown in Fig. 5(b) as gray isosurfaces at $|\langle\hat{\mathbf{F}}\rangle|^2 = 1$. This reflection of the order-parameter symmetry in the core on the spatial symmetry of the defect core itself is known to appear in the cyclic core of a BN HQV as a result of joining the mismatched point-group symmetries of the core and bulk superfluid [41,97]. In Fig. 5(b), we illustrate the relaxed monopole state using two intersecting planes slicing, respectively, through and between the FM regions.

V. CONCLUSIONS

In summary, we have demonstrated that a topological point defect in the UN phase of a spin-2 BEC relaxes to form a spin-Alice ring with a composite-defect core structure consisting of a BN outer core exhibiting a spin HQV surrounding a UN inner core that accommodates the line singularity. By numerical simulation, we have further shown that the spin-Alice ring exhibits dynamic oscillations between the Alice-ring state and a state corresponding to a split-core monopole configuration analogous to corresponding states in field theories [21] and liquid crystals [72,73], all while preserving the overall monopole topological (Cheshire) charge. The core oscillations are characterized by the appearance of FM rings with associated mass circulation inside the extended monopole core. In addition, we have also considered monopoles in the BN and cyclic phases, where the second homotopy group is trivial, but states similar to Dirac monopoles, with associated singular line defects, are still possible. We have shown that a BN monopole situated on a spin vortex, which relaxes to a

BN spin-Alice ring surrounding the vortex line [41], exhibits a similar oscillatory behavior between spin-Alice-ring and split-core configurations as the true point defect in the UN case. A similar monopole configuration in the cyclic phase, by contrast, does not lead to Alice-ring formation, but we instead find the appearance of an extended core containing FM rings with fractional mass circulation. When the cyclic monopole instead forms the termination point of a spin vortex, energy relaxation leads to the formation of a composite core whose spatial symmetry reflects the order-parameter symmetry of a cyclic-phase inner monopole core.

Alice rings have recently been experimentally observed in a spin-1 BEC [63]. In this experiment, the initial monopole state was prepared using the magnetic-field imprinting method proposed in Ref. [5] and previously used to prepare monopole [6,17], knot [59], and skyrmion [55] states in spin-1 condensates. Similar techniques, as well as other methods for engineering topological defects in spin-2 phases [58], can, in principle, enable the observation of the spin-Alice rings and the associated core dynamics.

The data used in this publication are available at [98].

[1] P. A. M. Dirac, Quantized Singularities in the Electromagnetic Field, Proc. R. Soc. London A **133**, 60 (1931).

[2] G. E. Volovik, Monopoles and fractional vortices in chiral superconductors, Proc. Natl. Acad. Sci. USA **97**, 2431 (2000).

[3] G. E. Volovik, *The Universe in a Helium Droplet* (Oxford University Press, Oxford, 2003).

[4] C. M. Savage and J. Ruostekoski, Dirac monopoles and dipoles in ferromagnetic spinor Bose-Einstein condensates, Phys. Rev. A **68**, 043604 (2003).

[5] V. Pietilä and M. Möttönen, Creation of Dirac monopoles in spinor Bose-Einstein condensates, Phys. Rev. Lett. **103**, 030401 (2009).

[6] M. W. Ray, E. Ruokokoski, S. Kandel, M. Möttönen, and D. S. Hall, Observation of Dirac monopoles in a synthetic magnetic field, Nature (London) **505**, 657 (2014).

[7] G.'T. Hooft, Magnetic monopoles in unified gauge theories, Nucl. Phys. B **79**, 276 (1974).

[8] A. M. Polyakov, Particle spectrum in quantum field theory, JETP Lett. **20**, 194 (1974).

[9] T. W. B. Kibble, Topology of cosmic domains and strings, J. Phys. A: Math. Gen. **9**, 1387 (1976).

[10] J. P. Preskill, Cosmological Production of Superheavy Magnetic Monopoles, Phys. Rev. Lett. **43**, 1365 (1979).

[11] E. J. Weinberg and P. Yi, Magnetic monopole dynamics, supersymmetry, and duality, Phys. Rep. **438**, 65 (2007).

[12] N. Schopohl and T. Sluckin, Hedgehog structure in nematic and magnetic systems, J. Phys. France **49**, 1097 (1988).

[13] H. Mori and H. Nakanishi, On the stability of topologically nontrivial point defects, J. Phys. Soc. Jpn. **57**, 1281 (1988).

[14] I. Chuang, R. Durrer, N. Turok, and B. Yurke, Cosmology in the laboratory: Defect dynamics in liquid crystals, Science **251**, 1336 (1991).

[15] H. T. C. Stoof, E. Vliegen, and U. Al Khawaja, Monopoles in an antiferromagnetic Bose-Einstein condensate, Phys. Rev. Lett. **87**, 120407 (2001).

[16] J. Ruostekoski and J. R. Anglin, Monopole core instability and alice rings in spinor Bose-Einstein condensates, Phys. Rev. Lett. **91**, 190402 (2003).

[17] M. W. Ray, E. Ruokokoski, K. Tiurev, M. Möttönen, and D. S. Hall, Observation of isolated monopoles in a quantum field, Science **348**, 544 (2015).

[18] N. D. Mermin, The topological theory of defects in ordered media, Rev. Mod. Phys. **51**, 591 (1979).

[19] T. Annala and M. Möttönen, Charge ambiguity and splitting of monopoles, Phys. Rev. Res. **4**, 023209 (2022).

[20] M. Bucher, H.-K. Lo, and J. Preskill, Topological approach to Alice electrodynamics, Nucl. Phys. B **386**, 3 (1992).

[21] F. A. Bais and J. Striet, On a core instability of 't Hooft-Polyakov type monopoles, Phys. Lett. B **540**, 319 (2002).

[22] M. G. Alford, K. Benson, S. Coleman, J. March-Russell, and F. Wilczek, Interactions and excitations of non-Abelian vortices, Phys. Rev. Lett. **64**, 1632 (1990).

[23] A. Schwarz, Field theories with no local conservation of the electric charge, Nucl. Phys. B **208**, 141 (1982).

[24] A. Schwarz and Y. Tyupkin, Grand unification and mirror particles, Nucl. Phys. B **209**, 427 (1982).

[25] G. Volovik and V. Mineev, Investigation of singularities in superfluid He^3 in liquid crystals by the homotopic topology methods, Sov. Phys. JETP **45**, 1186 (1977).

[26] K. A. Milton, Theoretical and experimental status of magnetic monopoles, Rep. Prog. Phys. **69**, 1637 (2006).

[27] Y. Kawaguchi and M. Ueda, Spinor Bose-Einstein condensates, Phys. Rep. **520**, 253 (2012).

[28] D. M. Stamper-Kurn and M. Ueda, Spinor Bose gases: Symmetries, magnetism, and quantum dynamics, Rev. Mod. Phys. **85**, 1191 (2013).

[29] M. Nakahara, T. Isoshima, K. Machida, S.-i. Ogawa, and T. Ohmi, A simple method to create a vortex in Bose–Einstein condensate of alkali atoms, Phys. B: Condens. Matter **284-288**, 17 (2000).

[30] T. Isoshima, M. Nakahara, T. Ohmi, and K. Machida, Creation of a persistent current and vortex in a bose-einstein condensate of alkali-metal atoms, Phys. Rev. A **61**, 063610 (2000).

[31] D. M. Stamper-Kurn, M. R. Andrews, A. P. Chikkatur, S. Inouye, H.-J. Miesner, J. Stenger, and W. Ketterle, Optical Confinement of a Bose-Einstein Condensate, Phys. Rev. Lett. **80**, 2027 (1998).

[32] M. Ueda, Topological aspects in spinor Bose-Einstein condensates, Rep. Prog. Phys. **77**, 122401 (2014).

[33] S.-K. Yip, Internal vortex structure of a trapped spinor Bose-Einstein condensate, Phys. Rev. Lett. **83**, 4677 (1999).

[34] T. Isoshima and K. Machida, Axisymmetric vortices in spinor Bose-Einstein condensates under rotation, Phys. Rev. A **66**, 023602 (2002).

[35] J. Lovegrove, M. O. Borgh, and J. Ruostekoski, Energetically stable singular vortex cores in an atomic spin-1 Bose-Einstein condensate, Phys. Rev. A **86**, 013613 (2012).

[36] U. Leonhardt and G. E. Volovik, How to create an Alice string (half-quantum vortex) in a vector Bose-Einstein condensate, JETP Lett. **72**, 46 (2000).

[37] F. Zhou, Quantum spin nematic states in Bose–Einstein condensates, Intl. J. Mod. Phys. B **17**, 2643 (2003).

[38] G. W. Semenoff and F. Zhou, Discrete symmetries and 1/3–quantum vortices in condensates of $F = 2$ cold atoms, Phys. Rev. Lett. **98**, 100401 (2007).

[39] J. A. M. Huhtamäki, T. P. Simula, M. Kobayashi, and K. Machida, Stable fractional vortices in the cyclic states of Bose-Einstein condensates, Phys. Rev. A **80**, 051601(R) (2009).

[40] M. Kobayashi, Y. Kawaguchi, M. Nitta, and M. Ueda, Collision dynamics and rung formation of non-Abelian vortices, Phys. Rev. Lett. **103**, 115301 (2009).

[41] M. O. Borgh and J. Ruostekoski, Core structure and non-Abelian reconnection of defects in a biaxial nematic spin-2 Bose-Einstein condensate, Phys. Rev. Lett. **117**, 275302 (2016).

[42] T. Mizushima, K. Machida, and T. Kita, Mermin-Ho vortex in ferromagnetic spinor Bose-Einstein condensates, Phys. Rev. Lett. **89**, 030401 (2002).

[43] J.-P. Martikainen, A. Collin, and K.-A. Suominen, Coreless vortex ground state of the rotating spinor condensate, Phys. Rev. A **66**, 053604 (2002).

[44] T. Mizushima, N. Kobayashi, and K. Machida, Coreless and singular vortex lattices in rotating spinor Bose-Einstein condensates, Phys. Rev. A **70**, 043613 (2004).

[45] U. Al Khawaja and H. Stoof, Skyrmions in a ferromagnetic Bose-Einstein condensate, Nature (London) **411**, 918 (2001).

[46] J. Ruostekoski and J. R. Anglin, Creating vortex rings and three-dimensional skyrmions in Bose-Einstein condensates, Phys. Rev. Lett. **86**, 3934 (2001).

[47] R. A. Battye, N. R. Cooper, and P. M. Sutcliffe, Stable skyrmions in two-component Bose-Einstein condensates, Phys. Rev. Lett. **88**, 080401 (2002).

[48] C. M. Savage and J. Ruostekoski, Energetically stable particlelike skyrmions in a trapped Bose-Einstein condensate, Phys. Rev. Lett. **91**, 010403 (2003).

[49] K. Tiurev, T. Ollikainen, P. Kuopanportti, M. Nakahara, D. S. Hall, and M. Möttönen, Three-dimensional skyrmions in spin-2 Bose–Einstein condensates, New J. Phys. **20**, 055011 (2018).

[50] L. E. Sadler, J. M. Higbie, S. R. Leslie, M. Vengalattore, and D. M. Stamper-Kurn, Spontaneous symmetry breaking in a quenched ferromagnetic spinor Bose–Einstein condensate, Nature (London) **443**, 312 (2006).

[51] S. W. Seo, S. Kang, W. J. Kwon, and Y. I. Shin, Half-quantum vortices in an antiferromagnetic spinor Bose-Einstein condensate, Phys. Rev. Lett. **115**, 015301 (2015).

[52] A. E. Leanhardt, Y. Shin, D. Kielpinski, D. E. Pritchard, and W. Ketterle, Coreless vortex formation in a spinor Bose-Einstein condensate, Phys. Rev. Lett. **90**, 140403 (2003).

[53] J.-Y. Choi, W. J. Kwon, and Y.-I. Shin, Observation of topologically stable 2D Skyrmions in an antiferromagnetic spinor Bose-Einstein condensate, Phys. Rev. Lett. **108**, 035301 (2012).

[54] J.-Y. Choi, W. J. Kwon, M. Lee, H. Jeong, K. An, and Y.-I. Shin, Imprinting Skyrmion spin textures in Bose–Einstein condensates, New J. Phys. **14**, 053013 (2012).

[55] W. Lee, A. H. Gheorghe, K. Tiurev, T. Ollikainen, M. Möttönen, and D. S. Hall, Synthetic electromagnetic knot in a three-dimensional Skyrmion, Sci. Adv. **4**, eaao3820 (2018).

[56] L. S. Weiss, M. O. Borgh, A. Blinova, T. Ollikainen, M. Möttönen, J. Ruostekoski, and D. S. Hall, Controlled creation of a singular spinor vortex by circumventing the Dirac belt trick, Nat. Commun. **10**, 4772 (2019).

[57] Y. Xiao, M. O. Borgh, L. S. Weiss, A. A. Blinova, J. Ruostekoski, and D. S. Hall, Controlled creation and decay of singly-quantized vortices in a polar magnetic phase, Commun. Phys. **4**, 52 (2021).

[58] Y. Xiao, M. O. Borgh, A. Blinova, T. Ollikainen, J. Ruostekoski, and D. S. Hall, Topological superfluid defects with discrete point group symmetries, Nat. Commun. **13**, 4635 (2022).

[59] D. S. Hall, M. W. Ray, K. Tiurev, E. Ruokokoski, A. H. Gheorghe, and M. Möttönen, Tying quantum knots, Nat. Phys. **12**, 478 (2016).

[60] M. Jayaseelan, J. D. Murphree, J. T. Schultz, J. Ruostekoski, and N. P. Bigelow, Topological atom optics and beyond with knotted quantum wave functions, Commun. Phys. **7**, 7 (2024).

[61] C. D. Parmee, M. R. Dennis, and J. Ruostekoski, Optical excitations of Skyrmions, knotted solitons, and defects in atoms, Commun. Phys. **5**, 54 (2022).

[62] T. Ollikainen, K. Tiurev, A. Blinova, W. Lee, D. S. Hall, and M. Möttönen, Experimental realization of a Dirac monopole through the decay of an isolated monopole, Phys. Rev. X **7**, 021023 (2017).

[63] A. Blinova, R. Zamora-Zamora, T. Ollikainen, M. Kivioja, M. Möttönen, and D. S. Hall, Observation of an Alice ring in a Bose-Einstein condensate, Nat. Commun. **14**, 5100 (2023).

[64] H. Nakanishi, K. Hayashi, and H. Mori, Topological classification of unknotted ring defects, Commun. Math. Phys. **117**, 203 (1988).

[65] E. Ruokokoski, V. Pietilä, and M. Möttönen, Ground-state Dirac monopole, Phys. Rev. A **84**, 063627 (2011).

[66] K. Tiurev, E. Ruokokoski, H. Mäkelä, D. S. Hall, and M. Möttönen, Decay of an isolated monopole into a Dirac monopole configuration, Phys. Rev. A **93**, 033638 (2016).

[67] K. Tiurev, P. Kuopanportti, and M. Möttönen, Creation of a Dirac monopole-antimonopole pair in a spin-1 Bose-Einstein condensate, Phys. Rev. A **99**, 023621 (2019).

[68] T. Mithun, R. Carretero-González, E. G. Charalampidis, D. S. Hall, and P. G. Kevrekidis, Existence, stability, and dynamics of monopole and Alice ring solutions in antiferromagnetic spinor condensates, Phys. Rev. A **105**, 053303 (2022).

[69] M. Kivioja, R. Zamora-Zamora, A. Blinova, S. Mönkölä, T. Rossi, and M. Möttönen, Evolution and decay of an Alice ring in a spinor Bose-Einstein condensate, Phys. Rev. Res. **5**, 023104 (2023).

[70] J. Lovegrove, M. O. Borgh, and J. Ruostekoski, Energetic stability of coreless vortices in spin-1 Bose-Einstein condensates with conserved magnetization, Phys. Rev. Lett. **112**, 075301 (2014).

[71] J. Lovegrove, M. O. Borgh, and J. Ruostekoski, Stability and internal structure of vortices in spin-1 Bose-Einstein condensates with conserved magnetization, Phys. Rev. A **93**, 033633 (2016).

[72] E. C. Gartland and S. Mkaddem, Instability of radial hedge-hog configurations in nematic liquid crystals under Landau–de Gennes free-energy models, Phys. Rev. E **59**, 563 (1999).

[73] S. Mkaddem and E. C. Gartland, Fine structure of defects in radial nematic droplets, Phys. Rev. E **62**, 6694 (2000).

[74] A. Corney, *Atomic and Laser Spectroscopy* (Oxford University Press, Oxford, 2006).

[75] M. Koashi and M. Ueda, Exact eigenstates and magnetic response of spin-1 and spin-2 Bose-Einstein condensates, Phys. Rev. Lett. **84**, 1066 (2000).

[76] F. Zhou, Spin correlation and discrete symmetry in spinor Bose-Einstein condensates, Phys. Rev. Lett. **87**, 080401 (2001).

[77] S. Kobayashi, M. Kobayashi, Y. Kawaguchi, M. Nitta, and M. Ueda, Abe homotopy classification of topological excitations under the topological influence of vortices, Nucl. Phys. B **856**, 577 (2012).

[78] J. L. Song, G. W. Semenoff, and F. Zhou, Uniaxial and Biaxial Spin Nematic Phases Induced by Quantum Fluctuations, Phys. Rev. Lett. **98**, 160408 (2007).

[79] S.-K. Yip, Symmetry and inert states of spin Bose-Einstein condensates, Phys. Rev. A **75**, 023625 (2007).

[80] M. Ueda and M. Koashi, Theory of spin-2 Bose-Einstein condensates: Spin correlations, magnetic response, and excitation spectra, Phys. Rev. A **65**, 063602 (2002).

[81] C. V. Ciobanu, S.-K. Yip, and T.-L. Ho, Phase diagrams of $F = 2$ spinor Bose-Einstein condensates, Phys. Rev. A **61**, 033607 (2000).

[82] N. N. Klausen, J. L. Bohn, and C. H. Greene, Nature of spinor Bose-Einstein condensates in rubidium, Phys. Rev. A **64**, 053602 (2001).

[83] A. Widera, F. Gerbier, S. Fölling, T. Gericke, O. Mandel, and I. Bloch, Precision measurement of spin-dependent interaction strengths for spin-1 and spin-2 ^{87}Rb atoms, New J. Phys. **8**, 152 (2006).

[84] A. M. Turner, R. Barnett, E. Demler, and A. Vishwanath, Nematic order by disorder in spin-2 Bose-Einstein condensates, Phys. Rev. Lett. **98**, 190404 (2007).

[85] W. Zhang, S. Yi, and L. You, Mean field ground state of a spin-1 condensate in a magnetic field, New J. Phys. **5**, 77 (2003).

[86] K. Murata, H. Saito, and M. Ueda, Broken-axisymmetry phase of a spin-1 ferromagnetic Bose-Einstein condensate, Phys. Rev. A **75**, 013607 (2007).

[87] H. Mäkelä, Y. Zhang, and K.-A. Suominen, Topological defects in spinor condensates, J. Phys. A: Math. Gen. **36**, 8555 (2003).

[88] G. Baio, M. T. Wheeler, D. S. Hall, J. Ruostekoski, and M. O. Borgh, Topological interfaces crossed by defects and textures of continuous and discrete point group symmetries in spin-2 Bose-Einstein condensates, Phys. Rev. Res. **6**, 013046 (2024).

[89] Y. Kawaguchi and M. Ueda, Symmetry classification of spinor Bose-Einstein condensates, Phys. Rev. A **84**, 053616 (2011).

[90] J. Javanainen and J. Ruostekoski, Symbolic calculation in development of algorithms: Split-step methods for the Gross-Pitaevskii equation, J. Phys. A: Math. Gen. **39**, L179 (2006).

[91] S. Kralj, E. G. Virga, and S. Žumer, Biaxial torus around nematic point defects, Phys. Rev. E **60**, 1858 (1999).

[92] M. O. Borgh and J. Ruostekoski, Topological interface engineering and defect crossing in ultracold atomic gases, Phys. Rev. Lett. **109**, 015302 (2012).

[93] M. O. Borgh, J. Lovegrove, and J. Ruostekoski, Imprinting a topological interface using Zeeman shifts in an atomic spinor Bose-Einstein condensate, New J. Phys. **16**, 053046 (2014).

[94] A. Villois, G. Krstulovic, D. Proment, and H. Salman, A vortex filament tracking method for the Gross–Pitaevskii model of a superfluid, J. Phys. A: Math. Theor. **49**, 415502 (2016).

[95] M. T. Wheeler, H. Salman, and M. O. Borgh, Relaxation dynamics of half-quantum vortices in a two-dimensional two-component Bose-Einstein condensate, Europhys. Lett. **135**, 30004 (2021).

[96] G. P. Alexander, Bryan Gin-ge Chen, E. A. Matsumoto, and R. D. Kamien, Colloquium: Disclination loops, point defects, and all that in nematic liquid crystals, Rev. Mod. Phys. **84**, 497 (2012).

[97] M. Kobayashi, Y. Kawaguchi, and M. Ueda, Vortex tiling in a spin-2 spinor Bose-Einstein condensate, arXiv:0907.3716.

[98] G. Baio and M. O. Borgh, Dataset from Composite cores of monopoles and Alice rings in spin-2 Bose-Einstein condensates, https://doi.org/10.5281/zenodo.10808073.